

Title	The multidrug-resistance transporter MdfA from Escherichia coli: crystallization and X-ray diffraction analysis
Author(s)	Nagarathinam, Kumar; Jaenecke, Frank; Nakada-Nakura, Yoshiko; Hotta, Yunhon; Liu, Kehong; Iwata, So; Stubbs, Milton T.; Nomura, Norimichi; Tanabe, Mikio
Citation	Acta Crystallographica Section F (2017), 73: 423-430
Issue Date	2017-7-1
URL	http://hdl.handle.net/2433/226310
Right	Copyright © International Union of Crystallography; Author(s) of this paper may load this reprint on their own web site or institutional repository provided that this cover page is retained. Republication of this article or its storage in electronic databases other than as specified above is not permitted without prior permission in writing from the IUCr.
Type	Journal Article
Textversion	publisher



The multidrug-resistance transporter MdfA from *Escherichia coli*: crystallization and X-ray diffraction analysis

Kumar Nagarathinam, Frank Jaenecke, Yoshiko Nakada-Nakura, Yunhon Hotta, Kehong Liu, So Iwata, Milton T. Stubbs, Norimichi Nomura and Mikio Tanabe

Acta Cryst. (2017). **F73**, 423–430



IUCr Journals
CRYSTALLOGRAPHY JOURNALS ONLINE

Copyright © International Union of Crystallography

Author(s) of this paper may load this reprint on their own web site or institutional repository provided that this cover page is retained. Republication of this article or its storage in electronic databases other than as specified above is not permitted without prior permission in writing from the IUCr.

For further information see <http://journals.iucr.org/services/authorrights.html>



The multidrug-resistance transporter MdfA from *Escherichia coli*: crystallization and X-ray diffraction analysis

Kumar Nagarathinam,^{a,b} Frank Jaenecke,^a Yoshiko Nakada-Nakura,^c Yunhon Hotta,^c Kehong Liu,^c So Iwata,^{c,d,e} Milton T. Stubbs,^{a,b} Norimichi Nomura^{c,d} and Mikio Tanabe^{a*‡}

Received 15 February 2017

Accepted 7 June 2017

Edited by A. Nakagawa, Osaka University, Japan

‡ Current and correspondence address: Structural Biology Research Center, Photon Factory, Institute of Materials Structure Science, High Energy Accelerator Research Organization (KEK), 1-1 Oho, Tsukuba, Ibaraki 305-0801, Japan.

Keywords: MFS transporter; multidrug resistance; membrane protein; crystallization; antibody fragment; lipidic cubic phase.

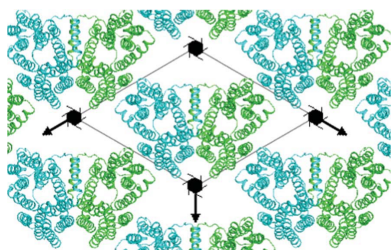
Supporting information: this article has supporting information at journals.iucr.org/f

^aZIK HALOmem, Martin-Luther-Universität Halle-Wittenberg, Kurt-Mothes Strasse 3, 06120 Halle (Saale), Germany, ^bInstitut für Biochemie und Biotechnologie, Martin-Luther-Universität Halle-Wittenberg, Kurt-Mothes Strasse 3, 06120 Halle (Saale), Germany, ^cDepartment of Cell Biology, Graduate School of Medicine, Kyoto University, Konoe-cho, Sakyo-ku, Kyoto 606-8501, Japan, ^dResearch Acceleration Program, Membrane Protein Crystallography Project, Japan Science and Technology Agency, Konoe-cho, Sakyo-ku, Kyoto 606-8501, Japan, and ^eSpring-8 Center, RIKEN, Sayo, Kohto 1-1-1, Hyogo 679-5148, Japan. *Correspondence e-mail: mikio.tanabe@kek.jp

The active efflux of antibiotics by multidrug-resistance (MDR) transporters is a major pathway of drug resistance and complicates the clinical treatment of bacterial infections. MdfA is a member of the major facilitator superfamily (MFS) from *Escherichia coli* and provides resistance to a wide variety of dissimilar toxic compounds, including neutral, cationic and zwitterionic substances. The 12-transmembrane-helix MdfA was expressed as a GFP-octahistidine fusion protein with a TEV protease cleavage site. Following tag removal, MdfA was purified using two chromatographic steps, complexed with a Fab fragment and further purified using size-exclusion chromatography. MdfA and MdfA–Fab complexes were subjected to both vapour-diffusion and lipidic cubic phase (LCP) crystallization techniques. Vapour-diffusion-grown crystals were of type II, with poor diffraction behaviour and weak crystal contacts. LCP lipid screening resulted in type I crystals that diffracted to 3.4 Å resolution and belonged to the hexagonal space group $P6_122$.

1. Introduction

Active efflux by multidrug-resistance (MDR) transporters is a major cause of bacterial resistance to many classes of antibiotics (Nikaido, 2009). MDR transporters can be classified into primary transporters [such as ATP-binding cassette (ABC) transporters] that utilize ATP hydrolysis as an energy source, and secondary transporters, which utilize the energy stored in the transmembrane electrochemical gradient. On the basis of similarities in their sequences, the secondary transporters are further categorized into at least four large superfamilies, including the major facilitator superfamily (MFS), the resistance–nodulation–division (RND) family, the multidrug and toxic compounds extrusion (MATE) family and the small multidrug-resistance (SMR) family (Putman *et al.*, 2000). Proteins belonging to the MFS play a major role in prokaryotic MDR, yet the mechanism of drug transport is not entirely clear. The current accepted paradigm is that MFS transporters utilize a ‘rocker-switch alternating access’ mechanism, whereby the N-terminal and C-terminal six-helix bundles rotate with respect to each other about an axis within the plane of the membrane that passes through the central substrate-binding site. This mechanism requires at least three states: inward open, outward open and a (potentially



© 2017 International Union of Crystallography

transient) occluded form that may be further divided into inward and outward occluded states (Yan, 2013; Quistgaard *et al.*, 2016).

Sequence analysis of *Escherichia coli* MdfA suggested the presence of 12 transmembrane (TM) helices, a hallmark of the MFS (Edgar & Bibi, 1997; Sigal *et al.*, 2006), which was confirmed by the recent crystal structures of ligand-bound forms of MdfA in the inward-facing state (Heng *et al.*, 2015; Liu *et al.*, 2016). MdfA is capable of coupling the efflux of a number of lipophilic cationic, zwitterionic and neutral substrates to the transmembrane proton (H^+) or ion chemical gradient, allowing it to translocate antibiotics such as chloramphenicol, erythromycin, ethidium, tetraphenylphosphonium and rhodamine (Edgar & Bibi, 1997). A second physiological function of MdfA is found in pH regulation owing to its activity as an $H^+/Na^+,K^+$ antiporter: knockout of MdfA results in bacterial growth restriction under strongly alkaline conditions (Lewinson *et al.*, 2004).

Although MdfA can transport many structurally unrelated compounds, it has been suggested that similar conformations of the transporter are induced by the different permeant substrates (Fluman *et al.*, 2009), implying a common transport mechanism within the framework of the rocker-switch model. Two negatively charged residues located in TM helix 1 (Glu26 and Asp34) have been identified as playing critical roles in substrate and proton transport (Edgar & Bibi, 1999; Fluman *et al.*, 2012). The postulated transport mechanism involves competition between proton and substrate binding at these two acidic residues in the binding cavity of MdfA. Specifically, Asp34 is proposed to be involved in both proton and substrate binding (supported by the chloramphenicol-bound structure; Heng *et al.*, 2015), while protonation of Glu26 is thought to shift the conformation of the transporter from the outward open state to the inward open state; interplay between these two sites is thought to drive transport (Fluman *et al.*, 2012).

For a complete understanding of substrate binding and the transport mechanism, it is essential to identify and visualize additional conformational states of MdfA. Key prerequisites for structural analysis include homogenous and stable MdfA, yet such preparations remain a challenge for membrane proteins, which often suffer from poor expression levels and loss of activity after extraction from their native membranes by detergents. In addition, the resulting detergent micelle surrounding the protein may hamper the protein crystallization process and impact on the diffraction quality of membrane-protein crystals. Co-crystallization of membrane proteins with antibody fragments has been reported to be an effective means of improving the diffraction quality of membrane-protein crystals by limiting intrinsic flexibility. In addition, antibody binding increases the surface area exposed from detergent micelles, which is often thought to be critical for producing crystal contacts (Hino *et al.*, 2013).

Prior to this study, we expressed and purified the MFS-type MDR transporter MdfA from *E. coli* to generate and isolate antibody Fab fragments against MdfA, with a view towards using these as potential crystallization chaperones (Hino *et al.*, 2013). In this way, we were able to identify Fab fragments that

stabilize MdfA as measured using the *N*-[4-(7-diethylamino-4-methyl-3-coumarinyl)phenyl]maleimide (CPM) thermostability assay (Jaenecke *et al.*, 2017). Here, we show that the Fab fragment YN1074 is also able to suppress pH-dependent stability changes in the transporter. The MdfA–YN1074 complex could be crystallized using both hanging-drop vapour-diffusion and lipidic cubic phase (LCP) methods, and we demonstrate that lipid screening has a significant effect on the quality of crystals grown using LCP. The best crystals grew in LCP using the lipid 1-(8*Z*-hexadecenoyl)-*rac*-glycerol (8.8 MAG) and diffracted to a maximum resolution of 3.4 Å.

2. Materials and methods

2.1. Macromolecule production

2.1.1. Materials. All general reagents and materials were purchased from Sigma–Aldrich and Carl Roth, unless otherwise specified. Ni^{2+} –NTA resin was purchased from Qiagen. The detergents *n*-dodecyl- β -D-maltopyranoside (DDM), *n*-decyl- β -D-maltopyranoside (DM), *n*-nonyl- β -D-maltopyranoside (NM) and lauryl maltose neopentyl glycol (LMNG) were obtained from Anatrace (Maumee, Ohio, USA). Monoolein was obtained from Nu-Chek Prep (Elysian, Minnesota, USA) and other MAGs were purchased from Avanti Polar lipids (Alabaster, Alabama, USA). Polyethylene glycols (PEGs) for crystallization were obtained from Molecular Dimensions, whereas other materials for crystallization were obtained from Jena Biosciences, Hampton Research and Rigaku Reagents.

2.1.2. Cloning of MdfA. The *mdfA* gene (NCBI GenBank accession No. AAC73929.1 for *E. coli* K-12 substrain MG1655) was amplified from *E. coli* Top10 cells and cloned upstream of the TEV cleavage-site sequence (TEVcs) of pWaldo-GFPe (Drew *et al.*, 2001) via the XhoI and KpnI restriction sites, allowing expression of the MdfA-(TEVcs)-GFP-His₈ fusion protein. Two nucleotides were introduced between the gene sequences of *mdfA* and the TEVcs by site-directed mutagenesis in order to ensure the correct reading frame, using the oligonucleotides 5'-TCGCACGAAGGGG-GTACCTATGGATCCGAAAACCTGTAC-3' and 5'-GTA-CAGGTTTTTCGGATCCATAGGTACCCCCTTCGTGCGA-3'. *E. coli* C43 (DE3) cells were transformed with this plasmid and used for overexpression of the MdfA-(TEVcs)-GFP fusion protein.

2.1.3. MdfA expression and purification. A single colony was inoculated into LB medium containing kanamycin (75 μ g ml⁻¹) at 37°C overnight. The overnight culture was diluted (1:100; an OD₆₀₀ of approximately ~0.05) in 2× YT medium supplemented with kanamycin and the cells were grown at 37°C to an optical density (OD₆₀₀) of ~0.4. The temperature was decreased to 28°C and expression of the protein was induced by the addition of 0.4 mM IPTG. Cells were harvested 6 h after induction by centrifugation at 5000g for 10 min at 4°C.

The cell pellets were resuspended in 20 mM Tris pH 7.5, 150 mM NaCl, 5 mM EDTA buffer supplemented with

10 $\mu\text{g ml}^{-1}$ DNaseI, 1 mM PMSF and then disrupted by high-pressure homogenization (APV homogenizers). Cell debris was removed by centrifugation at 10 000g for 15 min, and the membrane fraction was collected by ultracentrifugation at 100 000g for 90 min. Isolated membranes were flash-frozen in liquid nitrogen and stored at -80°C . The membrane fraction was solubilized in 150 ml solubilization buffer (25 mM Tris, 200 mM NaCl pH 7.3) containing 1% DDM; the detergents DM, NM and LMNG were also screened, but only DDM yielded a monodisperse peak in SEC. Insoluble material was removed by centrifugation at 100 000g for 1 h and the solubilized fraction was incubated with 10 ml Ni^{2+} beads (batch binding) equilibrated in buffer A (20 mM Tris, 150 mM NaCl, 0.02% DDM pH 7.5) for 2 h. MdfA-GFP was purified by immobilized Ni^{2+} -affinity chromatography, with 0.02% DDM added to all buffers. The resin was washed with five column volumes (CV) of buffer A containing 20 mM imidazole, followed by 12 CV of buffer A containing 50 mM imidazole. MdfA-GFP was eluted with buffer A containing 250 mM imidazole, and fractions were pooled and exchanged with buffer A to reduce the concentration of imidazole (to ~ 10 mM) before treatment with TEV protease.

MdfA-GFP in the presence of a half-molar ratio of hexahistidine (His_6)-tagged TEV protease (Drew *et al.*, 2008) was dialyzed overnight against buffer A supplemented with 1 mM β -mercaptoethanol at 4°C using a 3 kDa molecular-weight cutoff membrane. After dialysis, the sample was passed through 15 ml Ni^{2+} -NTA resin equilibrated in dialysis buffer to separate the resulting MdfA (flowthrough) from the C-terminally His_8 -tagged GFP and the His_6 -tagged TEV protease. The fraction containing MdfA was concentrated and applied onto a Superdex 200 10/300 GL size-exclusion chromatography (SEC) column equilibrated with buffer B (10 mM MES, 20 mM NaCl, 0.02% DDM pH 7.0).

2.1.4. Preparation of Fab fragments. Fab fragments were generated as described previously (Jaenecke *et al.*, 2017; Supplementary Fig. S1) according to established protocols (Day *et al.*, 2007). Briefly, a proteoliposome antigen was prepared by reconstituting purified, functional MdfA at high density into phospholipid vesicles that consisted of a 10:1 mixture of egg phosphatidylcholine (Avanti Polar Lipids) and the adjuvant lipid A (Sigma) to facilitate the immune response. BALB/c mice were immunized with the proteoliposome antigen using three injections at two-week intervals. Antibody-producing hybridoma cell lines were generated using a conventional fusion protocol (Köhler & Milstein, 1975; Pontecorvo, 1976). Hybridoma clones producing antibodies against MdfA were selected by an enzyme-linked immunosorbent assay on immobilized phospholipid vesicles containing purified MdfA (liposome ELISA), allowing positive selection of those antibodies recognizing the native conformation of MdfA. Additional screening for reduced antibody binding to SDS-denatured MdfA was used to select against linear epitope-recognizing antibodies (negative selection). Whole IgG molecules, collected from large-scale culture supernatant of monoclonal hybridomas and purified using protein G affinity chromatography, were digested with papain (Nacalai) and

Fab fragments were isolated using a Superdex 200 gel-filtration column followed by protein A affinity chromatography (Bio-Rad). This procedure resulted in the isolation of four MdfA-specific monoclonal antibodies (YN1006, YN1010, YN1074 and YN1082), the Fab fragments of each of which form a stable complex with the transporter that can be isolated using SEC (Jaenecke *et al.*, 2017).

2.1.5. Preparation of MdfA–Fab fragment YN1074 complexes. Purified MdfA was incubated with Fab fragment YN1074 in a molar ratio of 1:1.5 for 16 h in buffer B prior to SEC. Peak fractions containing MdfA–YN1074 complexes were concentrated to ~ 5 mg ml^{-1} and used for crystallization. In a second set of experiments, the pH of buffer B during both MdfA–Fab complex formation and subsequent SEC and CPM thermostability assays was modified in the range between pH 5.5 and 7.0.

2.1.6. Thermostability assays of MdfA and the MdfA–Fab complex. CPM thermostability analysis was performed as described by Alexandrov *et al.* (2008) with minor modifications. Briefly, 12 μl MdfA or MdfA–Fab complex (2 mg ml^{-1}) was mixed with 45.6 μl buffer B and 2.4 μl CPM dye (at 5 mg ml^{-1}). The reaction mixture was transferred to a clean PCR tube and heated from 25 to 90°C at a rate of 1°C min^{-1} in a Rotor Gene Q cyclor (Qiagen). The fluorescence of the dye (excitation and emission wavelengths of 365 and 460 nm, respectively) was monitored during the heating process. Calculation of the first derivative of the melting curve (performed with the *Rotor Gene Q* software v.2.1.0) indicates a maximum at the apparent transition temperature/melting temperature T_m of the protein.

2.2. Crystallization

MdfA and the MdfA–YN1074 complex were concentrated to 5 and 2.5 mg ml^{-1} , respectively, using a 100 kDa molecular-weight cutoff Amicon (Millipore) prior to crystallization screening. Crystallization trials using the vapour-diffusion method were performed in 96-well sitting-drop plates using a Cartesian MicroSys NQ crystallization robot (Zinsser Analytic) with commercially available screening matrices (MemPlus and MemGold2 from Molecular Dimensions as well as Wizard I, II, III and IV from Rigaku Reagents). Droplets containing equal volumes of reservoir solution (200 nl) and protein solution (200 nl) were incubated against 70 μl of each reservoir solution at 16°C .

Initial LCP crystallization setups were made by mixing MdfA or the MdfA–YN1074 complex at 2.5, 5 or 10 mg ml^{-1} with monoolein acyl-glycerol (9.9 MAG) in a 2:3 ratio using the two-syringe coupling method (Caffrey & Cherezov, 2009). Protein-containing LCP (100 nl) was dispensed over each well of the Laminex glass plate (Molecular Dimensions) using a LISSYII robot (Zinsser Analytic) and overlaid with 1 μl precipitant solution from commercially available screening matrices (MemGold, MemGold2, MemStart+MemSys and MemMeso from Molecular Dimensions, JBScreen Membrane and JBScreen Pentaerythritol from Jena Bioscience, Crystal Screen HT, MemFac HT and Index HT from Hampton

Table 1
MdfA production information.

Source organism	<i>E. coli</i>
DNA source	<i>E. coli</i> Top10
Forward primer	AGGAGACTCGAGATGCAAAATAAATTAGCT
Reverse primer	TTTCGGATCCATAGGTACCCCTTCGTGCGAA
Expression vector	pWaldo-GFPe
Expression host	<i>E. coli</i> C43 (DE3)
Complete amino-acid sequence of the construct produced	MQNKLASGARLRGRQALLFPLCLVLYEFSTYIGNN- MIQPGMLAVVEQYQAGIDWVPTSMAYLAGGM- FLQWLLGPLSDRIGRRPVMLAGVWFIVTCLA- ILLAQNIEQFTLLRFLQGISLFCFIGAVGYAAI- QESFEEAVCIKITALMANVALIAPLLGPLVGA- AWIHVLPWEGMFVLAALAAISFFGLQRAMPE- TATRIGEKLSELKELGRDYKLVLNKGRFVAGAL- ALGFVSLPLLAWIAQSPIIIITGEQLSSYEYG- LLQVPIFGALIAGNLLARLTSRRTVRSLSIIM- GGWPIMIGLLVAAAATVISSHAYLWMTAGLSI- YAFGI LANAGLVRLTLFASDMSKGTVSAAMG- MLQMLIFTVGVIEISKHAWLNGGNLNFNLV- NGILWLSLMVIFLKDQKMGNSHEG

Research and Wizard 1 & 2 from Rigaku Reagents) for initial screening. Subsequently, the MAG lipids were varied for the MdfA–YN1074 complex using lipid mixing ratios of 1:1 {7.7 MAG [1-(7Z-tetradecenoyl)-*rac*-glycerol] and 7.8 MAG [1-(7Z-pentadecenoyl)-*rac*-glycerol]} and 2:3 {7.9 MAG [1-(7Z-hexadecenoyl)-*rac*-glycerol] and 8.8 MAG [1-(8Z-hexadecenoyl)-*rac*-glycerol]}. All crystallization trials were performed at 20°C.

2.3. Data collection and processing

Prior to data collection, single crystals of MdfA and the MdfA–YN1074 complex were harvested and flash-cooled directly in liquid nitrogen without additional cryoprotection. All data were collected on beamline PXI (X06SA) at the Swiss Light Source (SLS). For the MdfA and MdfA–YN1074 complex crystals grown using vapour diffusion, diffraction data sets were collected at 100 K using a PILATUS 6M detector, whereas diffraction data for the MdfA–YN1074 complex obtained from LCP were collected using an EIGER 16M detector. Diffraction data were processed and integrated using *XDS* (Kabsch, 2010). Molecular replacement was performed with *Phaser* (McCoy *et al.*, 2007) to analyse crystal packing using the coordinates of MdfA (PDB entry 4zp0; Heng *et al.*, 2015) and, where appropriate, a Fab fragment (PDB entry 1ibg; Jeffrey *et al.*, 1995) as search models (details of the structure solution and analysis will be presented elsewhere). Buried surface areas were calculated using the *PISA* server (Krissinel & Henrick, 2007) and crystallographic figures were prepared using *PyMOL* (Schrödinger).

3. Results and discussion

3.1. Cloning, expression and purification of MdfA

The PCR fragment coding for MdfA was successfully inserted into the *Xho*I and *Kpn*I sites of pWaldo-GFPe, which was then transformed into *E. coli* C43 (DE3) cells (Table 1). The expression level of MdfA-GFP was monitored by GFP fluorescence emission at 512 nm (excitation wavelength of

488 nm) using an ImageQuant LAS 4000 (GE Healthcare). Following isolation of MdfA-GFP by single-step immobilized metal-affinity chromatography (IMAC), untagged MdfA was obtained *via* TEV cleavage and a subsequent second IMAC step, resulting in >90% purity (Fig. 1). Approximately 0.3–0.4 mg of purified MdfA was routinely obtained from 1 l of 2 × YT medium.

3.2. Effect of Fab fragments on MdfA stability

At pH 7.0, the melting curve of MdfA shows an apparent transition temperature T_m of ~58°C in the CPM assay, which is increased by ~4°C in the complexes with Fabs YN1006, YN1010 and YN1082 and by ~12°C in the presence of Fab YN1074 (Jaenecke *et al.*, 2017). The thermostability of purified MdfA and the isolated MdfA–Fab YN1074 complex were

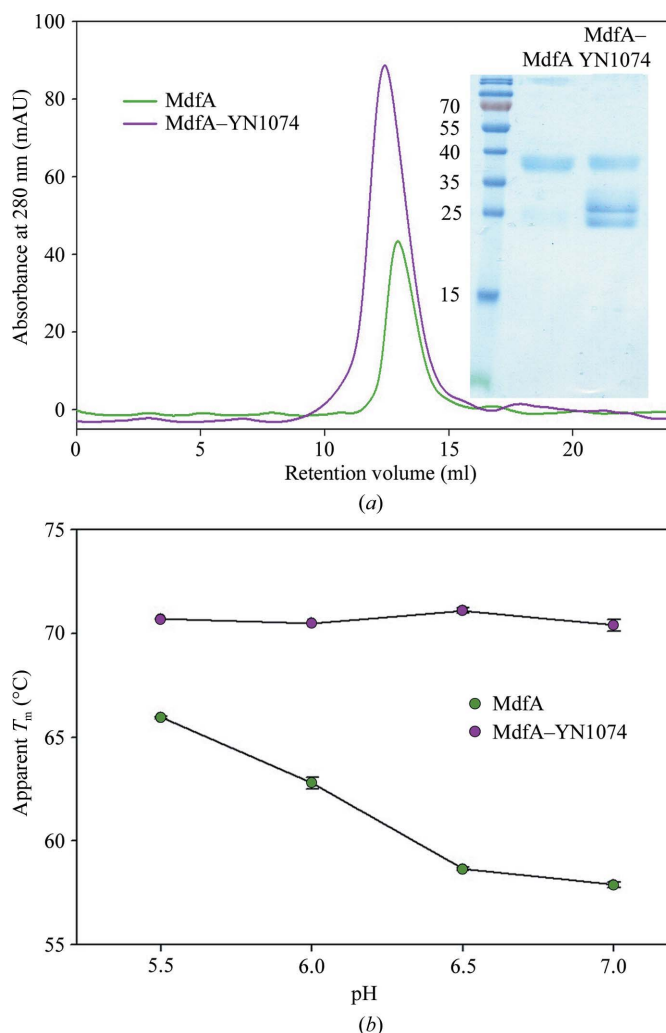


Figure 1
Purification of the MdfA–YN1074 complex and pH-dependent thermostability analyses of MdfA and the MdfA–YN1074 complex. (a) Size-exclusion chromatograms of MdfA (green) and MdfA–YN1074 (purple) on a Superdex 200 10/300 GL size-exclusion column. Inset: SDS-PAGE analysis of the main SEC peaks. (b) Thermostability of MdfA/the MdfA–YN1074 complex as a function of pH was assessed using the CPM thermal denaturation assay. Apparent T_m values for MdfA and the MdfA–YN1074 complex were evaluated from the first derivative of the melting curve.

Table 2
Crystallization of MdfA and MdfA–YN1074.

Protein	MdfA	MdfA–YN1074	MdfA–YN1074
Method	Hanging-drop vapour diffusion	Hanging-drop vapour diffusion	Lipidic cubic phase
Temperature (K)	289	289	293
Protein concentration (mg ml ⁻¹)	5	2.5	2.5
Buffer composition of protein solution	10 mM MES, 20 mM NaCl, 0.02% DDM pH 7.0	10 mM MES, 20 mM NaCl, 0.02% DDM pH 7.0	10 mM MES, 20 mM NaCl, 0.02% DDM pH 7.0
Composition of reservoir solution	100 mM Tris pH 7.5, 100 mM NaCl, 100 mM Li ₂ SO ₄ , 28–30% PEG 400	100 mM HEPES pH 7, 100 mM CdCl ₂ , 100 mM LiCl, 24–28% PEG 400	100 mM ADA pH 6.5, 100 mM NaCl, 100 mM Li ₂ SO ₄ , 32–36% PEG 300
Volume and ratio of drop	2 µl (1:1)	2 µl (1:1)	100 nl
Volume of reservoir	1 ml	1 ml	1 µl

further analysed as a function of pH (Fig. 1*b*). Interestingly, the antiporter exhibits an increased thermostability at lower pH values (T_m of $\sim 66^\circ\text{C}$ at pH 5.5). In contrast, the complex of MdfA with the YN1074 Fab possesses a near-constant T_m of $\sim 71^\circ\text{C}$ at all tested pH values, demonstrating a stabilization of MdfA by the Fab of 5–12°C. The lack of variation of the T_m of the complex with pH suggests that YN1074 stabilizes the low-pH form of the antiporter and that MdfA–YN1074 may be suitable for crystallization screening in a wide range of pH conditions.

3.3. Crystallization of MdfA

In the initial crystallization trials, we used commercially available screening kits with the sitting-drop vapour-diffusion method (Supplementary Fig. S1). Microcrystals of MdfA were observed after 1–2 weeks from a number of conditions containing PEG 400 as the precipitant (e.g. 0.1 M MES pH 6.0,

0.2 M Li₂SO₄, 25–30% PEG 400). These conditions were optimized to improve the crystal morphology using the hanging-drop vapour-diffusion method. The largest crystals were obtained in 100 mM Tris pH 7.5, 100 mM NaCl, 100 mM Li₂SO₄, 28–30% PEG 400 (MdfA–VD; Fig. 2*a*, Table 2), which diffracted to resolutions lower than 7 Å (Supplementary Fig. S2*a*). Processing of the diffraction data demonstrated that the MdfA–VD crystal belonged to the hexagonal space group $P6_122$ or $P6_522$, with unit-cell parameters $a = b = 94.5$, $c = 663.1$ Å (Table 3).

In parallel, crystallization conditions for MdfA in complex with the four Fabs were screened using vapour diffusion, and (with the exception of Fab YN1010) crystals were obtained (Supplementary Fig. S1). Nevertheless, the crystals of MdfA–YN1006 and MdfA–YN1082 diffracted poorly, with a maximum resolution of ~ 30 Å. Only those of the MdfA–YN1074 complex, obtained in 100 mM HEPES pH 7, 100 mM CdCl₂, 100 mM LiCl, 24–28% PEG 400 within 3–5 d

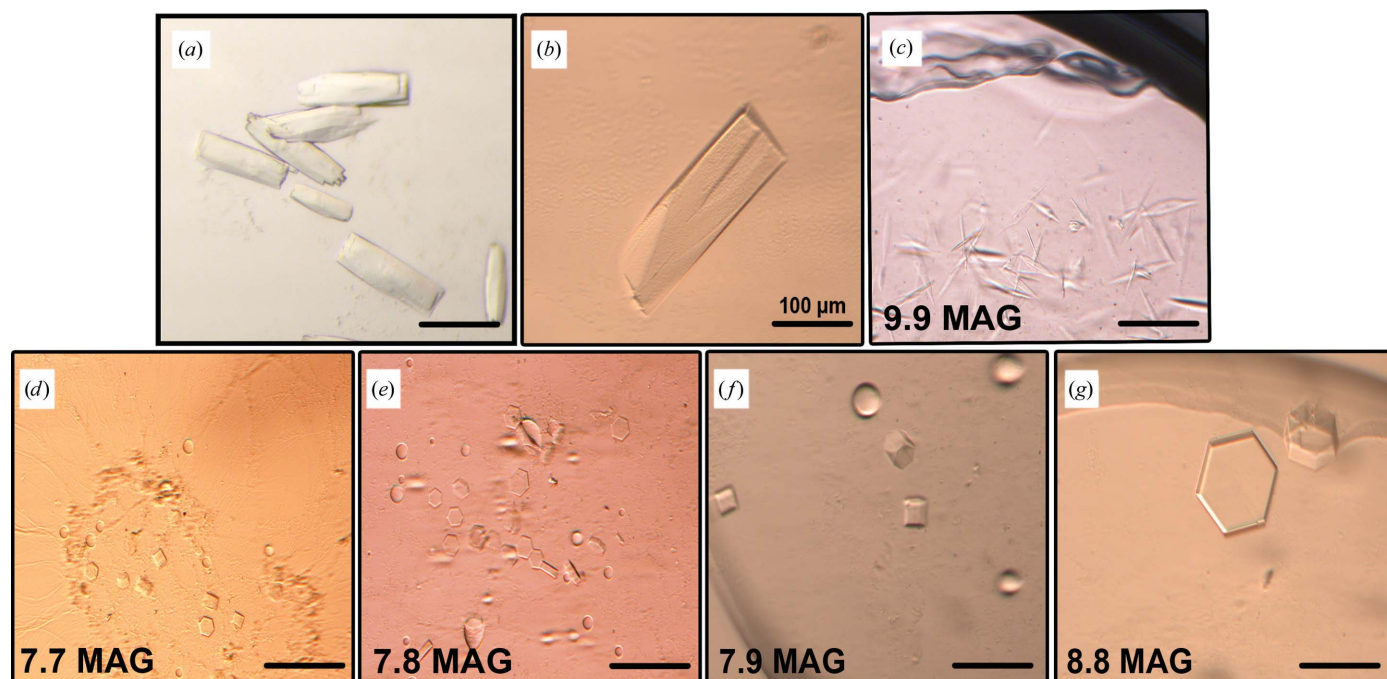


Figure 2
Crystals of MdfA and MdfA–YN1074. Crystals of (a) MdfA and (b) the MdfA–YN1074 complex grown by the hanging-drop vapour-diffusion method, as well as of the MdfA–YN1074 complex grown using the LCP method with various host lipids: (c) 9.9 MAG, (d) 7.7 MAG, (e) 7.8 MAG, (f) 7.9 MAG and (g) 8.8 MAG.

Table 3
Data collection and processing.

Values in parentheses are for the outer shell.

Protein	MdfA-VD (hanging-drop vapour diffusion)	MdfA-YN1074-VD (hanging-drop vapour diffusion)	MdfA-YN1074-LCP (lipidic cubic phase method)
Diffraction source	PXI (X06SA), SLS	PXI (X06SA), SLS	PXI (X06SA), SLS
Wavelength (Å)	1.000	1.000	1.000
Temperature (K)	100	100	100
Detector	PILATUS 6M	PILATUS 6M	EIGER 16M
Space group	$P6_522$	$P2_12_12_1$	$P6_122$
a, b, c (Å)	94.5, 94.5, 663.1	76.6, 141.6, 296.6	73.2, 73.2, 927.9
α, β, γ (°)	90, 90, 120	90, 90, 90	90, 90, 120
Resolution range (Å)	50–7.82 (8.28–7.82)	50–7.06 (7.48–7.06)	49–3.40 (3.61–3.40)
Total No. of reflections	39028	32684	384466
No. of unique reflections	3376	9469	22224
$CC_{1/2}$ (%)	100 (69.0)	99.9 (76.5)	100 (58.3)
R_{meas} (%)	9.7 (122.2)	6.0 (61.4)	26.2 (172.4)
$\langle I/\sigma(I) \rangle$	9.04 (1.65)	11.49 (2.01)	11.57 (1.59)†
Completeness (%)	99.1 (98.4)	98.3 (94.3)	99.9 (99.9)
Multiplicity	9.97 (9.77)	3.45 (3.44)	17.3 (16.03)
Mosaicity (°)	0.229	0.286	0.097
Solvent content (%)	74.5	71.6	68.1
No. of molecules/complexes per asymmetric unit	2	2	1

† The $\langle I/\sigma(I) \rangle$ falls below 2.0 at 3.4 Å resolution. The resolution cutoff was determined by the $CC_{1/2}$ value (Karplus & Diederichs, 2012), which is 58.3% (our cutoff value is below 50%).

(MdfA-YN1074-VD; Fig. 2*b*, Table 2), diffracted to a maximal resolution between 6 and 7 Å (Supplementary Fig. S2*b*). The MdfA-YN1074-VD crystal belonged to the orthorhombic space group $P2_12_12_1$, with unit-cell parameters $a = 76.6$, $b = 141.6$, $c = 296.6$ Å (Table 3).

The limitations in obtaining diffraction-quality crystals *via* the vapour-diffusion method prompted us to explore the lipidic cubic phase (LCP) technique. The LCP medium is ubiquitously used as an alternative to detergent micelles during the crystallization of membrane proteins (Caffrey, 2015). Needle-shaped crystals of the MdfA-YN1074 complex appeared in LCP using 9.9 MAG (the most frequently used host lipid in initial LCP trials; Caffrey, 2015) in 100 mM Tris pH 7.0, 100 mM NaCl, 100 mM Li_2SO_4 , 40–44% PEG 300 (Fig. 2*c*). These crystals, which belonged to the hexagonal space group $P6_122$ or $P6_522$, with unit-cell parameters $a = b = 73.3$, $c = 950.1$ Å, showed weak diffraction to 8 Å resolution.

We then screened the alkyl-chain length of the host lipid between 14-C and 18-C, which is thought to improve the partitioning of the membrane protein into the lipid and to influence the curvature of the bicontinuous lipidic bilayer to optimize the size of the aqueous channels to accommodate the bound Fab (Li *et al.*, 2013). Selection of lipids was informed empirically by reported membrane-protein structures grown by the LCP method (Caffrey, 2015). Crystallization in 7.7, 7.8 and 7.9 MAG generated small hexagonal crystals (<50 µm) in 100 mM ADA pH 6.5, 100 mM NaCl, 100 mM Li_2SO_4 , 24–26% PEG 300 (7.7 MAG), 100 mM ADA pH 6, 100 mM NaCl, 100 mM Li_2SO_4 , 28–30% PEG 300 (7.8 MAG) or 100 mM ADA pH 6.5, 100 mM NaCl, 100 mM Li_2SO_4 , 32–36% PEG 300 (7.9 MAG) (Figs. 2*d*, 2*e* and 2*f*), yet the diffraction quality remained limited.

Crystals grown in 8.8 MAG as a host lipid appeared within one week in 100 mM ADA pH 6.5, 100 mM NaCl, 100 mM

Li_2SO_4 , 32–36% PEG 300 and matured to full size within between five and seven weeks, when they were harvested (MdfA-YN1074-LCP; Fig. 2*g*, Table 2). The morphology of these larger crystals was hexagonal, and their maximal size was 80–100 µm. These crystals diffracted to a resolution of slightly over 3.0 Å (Supplementary Fig. S2*c*). Owing to the presence of a very long c axis, the crystals were mounted perpendicular to the beam with a slight tilt to best resolve the closely spaced diffraction spots. Anisotropy of the diffraction data restricted the resolution of the data set to 3.4 Å. The MdfA-YN1074-LCP crystal belonged to the hexagonal space group $P6_122$ or $P6_522$, with unit-cell parameters $a = b = 73.2$, $c = 927.9$ Å (*i.e.* related to those obtained using 9.9 MAG but with a 22 Å shorter c axis). Data-collection and processing statistics are summarized in Table 3.

The crystal packing in three of the crystal forms was analysed following molecular replacement (details of the structure solution and analysis will be presented elsewhere). Two MdfA molecules (solvent content of 74.5%) could be located in the asymmetric unit of the MdfA-VD crystal (Fig. 3*a*), two transporter–Fab complexes (solvent content of 71.6%) in that of MdfA-YN1074-VD (Figs. 3*b* and 3*c*) and one complex (solvent content 68.1%) in the asymmetric unit of MdfA-YN1074-LCP (Figs. 3*d* and 3*e*). In each crystal form, individual MdfA molecules associate laterally *via* their trans-membrane regions (although the residues that contact each other differ), with adjacent monomers facing in opposite directions (Fig. 3).

In the MdfA-VD crystal (Fig. 3*a*), hydrophobic TM-helix residues are responsible for most intermolecular contacts, with buried surface areas of 800 Å² between monomers within the asymmetric unit and 614 Å² between crystallographically related monomers. This results in the formation of super-helical ‘chains’ of MdfA molecules with their helix axes parallel to the crystallographic sixfold screw axis. The contacts

between adjacent chains, involving residues from the hydrophilic cytoplasmic and periplasmic surfaces of the transporter, are weak, burying a surface area of only 97 \AA^2 . The large spaces observed between the chains are presumably occupied by detergent micellar structures.

As expected, the intermolecular contacts in the MdfA–YN1074–VD crystal (Figs. 3*b* and 3*c*) are dominated by multiple Fab–Fab interactions, which bury a total surface area of 1179 \AA^2 . This is comparable to that of the MdfA–YN1074 interface (936 \AA^2). Lateral hydrophobic contacts between MdfA molecules are restricted to the interface within the asymmetric unit, with a buried surface area of 707 \AA^2 , whereas crystal contacts between the periplasmic faces of MdfA bury 307 \AA^2 . The complexes are arranged in rippled stacks within the crystals, with inter-stack contacts provided by the Fabs

(Fig. 3*c*). As in the MdfA–VD crystals, the interlayer spaces between MdfA molecules provide space for (presumably disordered) detergent.

In contrast to the type II membrane-protein crystals formed using vapour diffusion, the MdfA–YN1074–LCP crystal is of type I, with the MdfA molecules forming an infinite two-dimensional array as in a membrane, albeit with alternate facing monomers (Figs. 3*d* and 3*e*). Within this two-dimensional layer, two sets of lateral hydrophobic contacts are made, burying 1189 and 768 \AA^2 . Alternate layers are connected by Fab–Fab interactions that bury a total surface area of 900 \AA^2 . The favourable partitioning of intramembrane and hydrophilic contacts observed in the packing of these crystals is presumably responsible for their superior diffraction qualities.

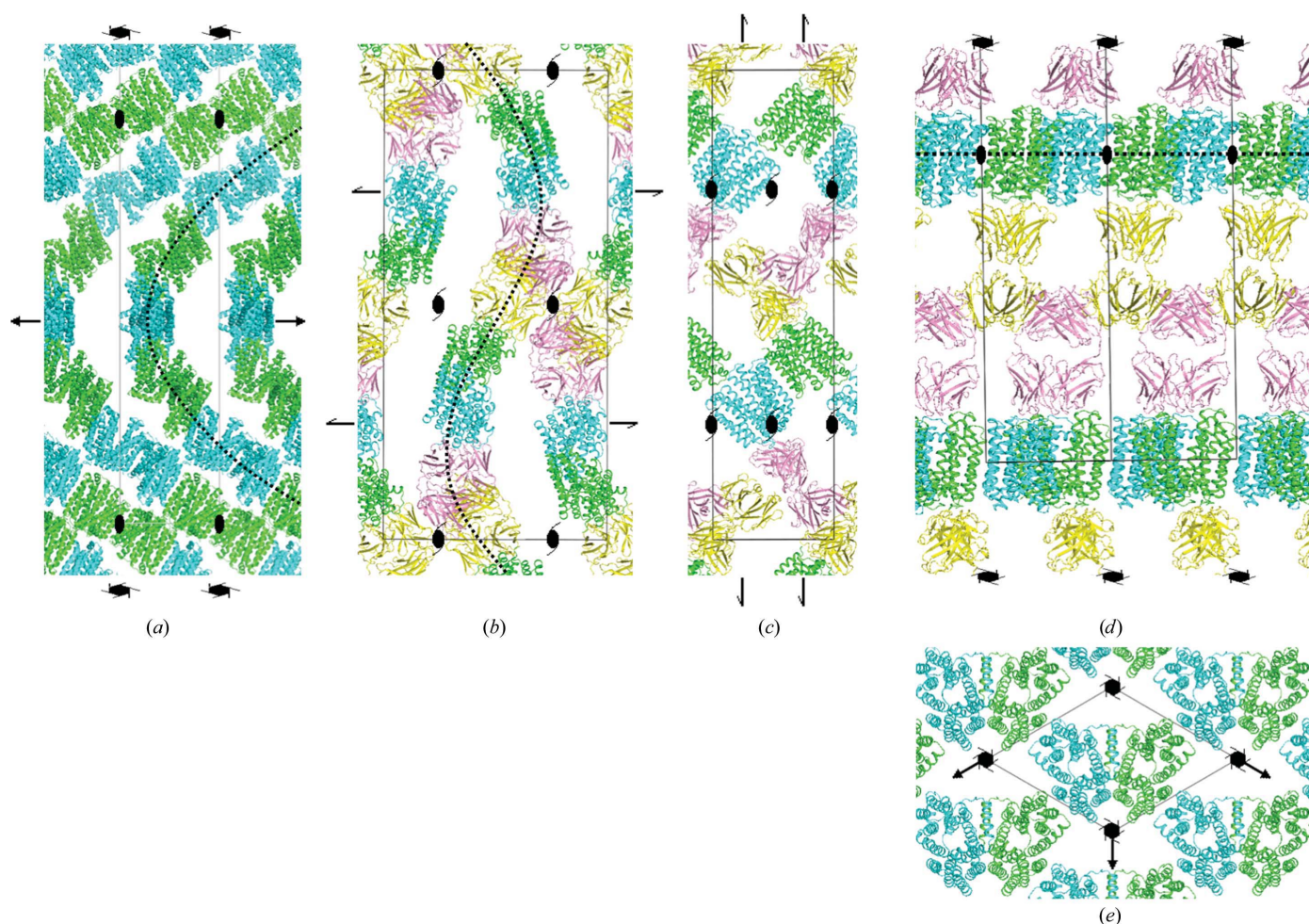


Figure 3

Crystal packing in MdfA crystals. Packing arrangements of (a) the transporter (MdfA–VD), (b, c) the MdfA–YN1074 complex within vapour-diffusion-grown (MdfA–YN1074–VD) crystals and (d, e) the MdfA–YN1074 membrane-protein complex within lipidic cubic phase-grown crystals (MdfA–YN1074–LCP). Selected symmetry-element symbols are shown for orientation. (a) The two MdfA monomers (green, cyan) within the asymmetric unit of MdfA–VD align to form infinite superhelical chains (dotted line) that are stabilized by lateral hydrophobic contacts. Individual chains contact each other *via* a small number of hydrophilic contacts. View parallel to the crystallographic *a* axis. (b) Crystal contacts in MdfA–YN1074–VD are dominated by interactions between the Fabs (yellow, pink) from symmetry-related molecules. Within the lattice, the molecules are arranged in rippled layers (dotted line), with major contacts between the layers provided by the Fabs. The view is parallel to the crystallographic *a* axis. (c) One layer from (b), viewed parallel to the crystallographic *b* axis. (d) In the MdfA–YN1074–LCP crystals, MdfA (green; for clarity, twofold symmetry-related molecules are shown in cyan, although these are crystallographically equivalent) is found in a two-dimensional membrane-like array. MdfA layers sandwich those of the Fab YN1074 (yellow; pink), resulting in a favourable segregation of hydrophobic and hydrophilic crystal contacts. The view is parallel to the crystallographic *a* axis. (e) The MdfA layer from (d), viewed parallel to the crystallographic *c* axis.

Although the data presented here by no means present a complete picture of the membrane-protein crystallization process, some conclusions may be drawn. Thus, it seems that the lipidic cubic phase facilitates optimal lateral contacts between membrane-protein molecules, supported by the fact that type I crystal formation appears to be typical for crystals obtained in LCP (Caffrey, 2015). In contrast, the arrangements in the vapour-diffusion crystals suggest that masking of the hydrophobic membrane-facing surfaces by detergent molecules prevents such two-dimensional arrangements. Coupled with the need to accommodate bulky disordered detergent micellar structures within the lattice, this results in weak crystal contacts and therefore poor diffraction. As observed previously (Hino *et al.*, 2013), complexation with antibody fragments can (in addition to stabilizing a particular conformation in flexible membrane proteins) increase the likelihood of obtaining three-dimensional crystals. In our case, however, it appears that Fab crystal contacts should be balanced by favourable membrane-protein interactions within the lattice for suitable diffraction properties, as observed in our LCP-grown crystals. Finally, the nature of the host lipid exhibits a pronounced influence both on the morphology and the diffraction quality of the LCP crystals. The fact that we observe a substantial change in the *c* axis for crystals grown using 8.8 MAG and 9.9 MAG suggests that the different lipids influence the two-dimensional packing of the membrane-protein layer and/or the orientation of the MdfA molecules, in turn influencing the positioning of the Fabs and allowing optimization of the crystal packing and diffraction quality.

Structural analyses of MdfA will be presented elsewhere.

Acknowledgements

We thank Martin Caffrey and Dianfan Li for advice concerning the LCP crystallization method, Christoph Parthier for assistance in data reduction and Tina Iverson for critically reading the manuscript. Crystallographic data were collected at the Swiss Light Source (SLS), Villigen with support from the European Community's 7th Framework Programme (FP7/2007-2013) under BioStruct-X (grant agreement No. 283570). The authors declare no conflict of interest.

Funding information

Funding for this research was provided by: Bundesministerium für Bildung und Forschung (BMBF) (ZIK program, award No. FKZ 03Z2HN21 to MT); ERDF (award No. 1241090001 to MTS); the Platform Project for Support in Drug Discovery and Life Science Research (Platform for Drug Discovery, Informatics and Structural Life Science) from the Japan Agency for Medical Research and Development

(AMED) to SI, NN and MT; the ERATO Human Receptor Crystallography Project of the Japan Science and Technology Agency (JST) to SI; the Strategic Basic Research Program, JST to SI and NN; the Research Acceleration Program of the JST to SI and NN; the Targeted Proteins Research Program of the Ministry of Education, Culture, Sports, Science and Technology (MEXT) of Japan to SI; Grants-in-Aids for Scientific Research from the MEXT (award No. 22570114 to NN); BioStruct-X (award Nos. 5450 and 8015 to MT).

References

- Alexandrov, A. I., Mileni, M., Chien, E. Y. T., Hanson, M. A. & Stevens, R. C. (2008). *Structure*, **16**, 351–359.
- Caffrey, M. (2015). *Acta Cryst.* **F71**, 3–18.
- Caffrey, M. & Cherezov, V. (2009). *Nature Protoc.* **4**, 706–731.
- Day, P. W., Rasmussen, S. G. F., Parnot, C., Fung, J. J., Masood, A., Kobilka, T. S., Yao, X.-J., Choi, H.-J., Weis, W. I., Rohrer, D. K. & Kobilka, B. K. (2007). *Nature Methods*, **4**, 927–929.
- Drew, D., Newstead, S., Sonoda, Y., Kim, H., von Heijne, G. & Iwata, S. (2008). *Nature Protoc.* **3**, 784–798.
- Drew, D. E., von Heijne, G., Nordlund, P. & de Gier, J. W. (2001). *FEBS Lett.* **507**, 220–224.
- Edgar, R. & Bibi, E. (1997). *J. Bacteriol.* **179**, 2274–2280.
- Edgar, R. & Bibi, E. (1999). *EMBO J.* **18**, 822–832.
- Fluman, N., Cohen-Karni, D., Weiss, T. & Bibi, E. (2009). *J. Biol. Chem.* **284**, 32296–32304.
- Fluman, N., Ryan, C. M., Whitelegge, J. P. & Bibi, E. (2012). *Mol. Cell*, **47**, 777–787.
- Heng, J., Zhao, Y., Liu, M., Liu, Y., Fan, J., Wang, X., Zhao, Y. & Zhang, X. C. (2015). *Cell Res.* **25**, 1060–1073.
- Hino, T., Iwata, S. & Murata, T. (2013). *Curr. Opin. Struct. Biol.* **23**, 563–568.
- Jaenecke, F., Nakada-Nakura, Y., Nagarathinam, K., Ogasawara, S., Liu, K., Hotta, Y., Iwata, S., Nomura, N. & Tanabe, M. (2017). In the press.
- Jeffrey, P. D., Schilbach, J. F., Chang, C. Y., Kussie, P. H., Margolies, M. N. & Sheriff, S. J. (1995). *J. Mol. Biol.* **248**, 344–360.
- Kabsch, W. (2010). *Acta Cryst.* **D66**, 125–132.
- Karplus, P. A. & Diederichs, K. (2012). *Science*, **336**, 1030–1033.
- Köhler, G. & Milstein, C. (1975). *Nature (London)*, **256**, 495–497.
- Krissinel, E. & Henrick, K. (2007). *J. Mol. Biol.* **372**, 774–797.
- Lewinson, O., Padan, E. & Bibi, E. (2004). *Proc. Natl Acad. Sci. USA*, **101**, 14073–14078.
- Li, D., Shah, S. T. A. & Caffrey, M. (2013). *Cryst. Growth Des.* **13**, 2846–2857.
- Liu, M., Heng, J., Gao, Y. & Wang, X. (2016). *Biophys. Rep.* **2**, 78–85.
- McCoy, A. J., Grosse-Kunstleve, R. W., Adams, P. D., Winn, M. D., Storoni, L. C. & Read, R. J. (2007). *J. Appl. Cryst.* **40**, 658–674.
- Nikaido, H. (2009). *Annu. Rev. Biochem.* **78**, 119–146.
- Pontecorvo, G. (1976). *Birth Defects Orig. Artic. Ser.* **12**, 399–400.
- Putman, M., van Veen, H. W. & Konings, W. N. (2000). *Microbiol. Mol. Biol. Rev.* **64**, 672–693.
- Quistgaard, E. M., Löw, C., Guettou, F. & Nordlund, P. (2016). *Nature Rev. Mol. Cell Biol.* **17**, 123–132.
- Sigal, N., Cohen-Karni, D., Siemion, S. & Bibi, E. (2006). *J. Mol. Microbiol. Biotechnol.* **11**, 308–317.
- Yan, N. (2013). *Trends Biochem. Sci.* **38**, 151–159.

Supporting Information

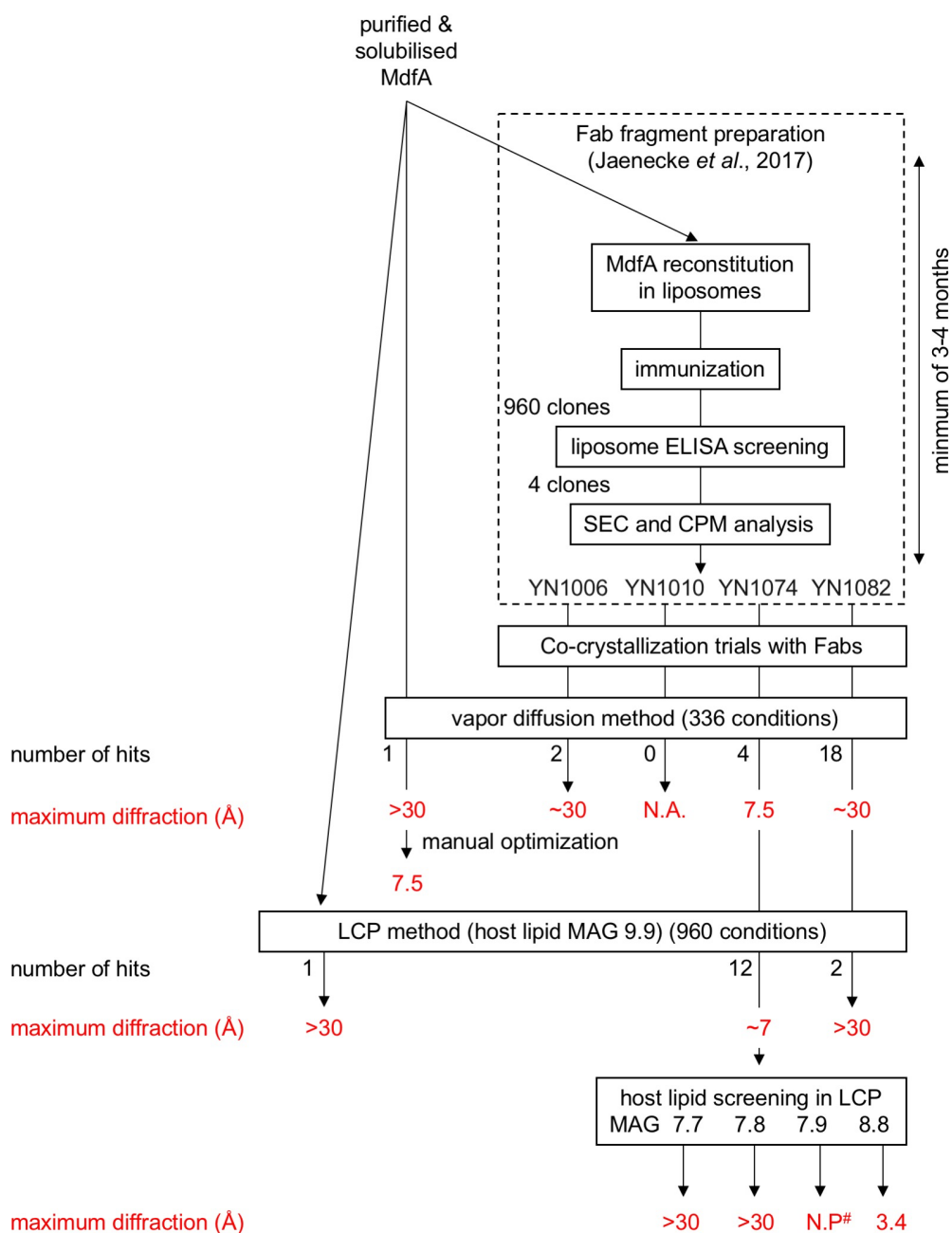


Fig. S1. Flowchart for crystallization of MdfA. The diagram provides a summary of the strategy for generating and optimizing MdfA crystals used in this study. The contribution of Fab for crystallization trials of MdfA were analyzed by 96-well formatted sitting-drop vapor diffusion method. The commercial available screens MemGold2, MemPlus, Wizard I & II, and Wizard III & IV were tested for initial screening for vapor diffusion crystallization trials (336 crystallization conditions in total). MemGold, MemGold2, MemStart & MemSys, MemMeso, JBScreen Membrane, and JBScreen Pentaerythritol, Crystal screen HT, MemFac HT, Index HT and Wizard I & II, were tested for LCP crystallization method (960 crystallization conditions in total). #N.P represents the crystal diffracted more than 7-8 Å (likely 5-6Å) but not processible, because of weak and smear diffraction images.

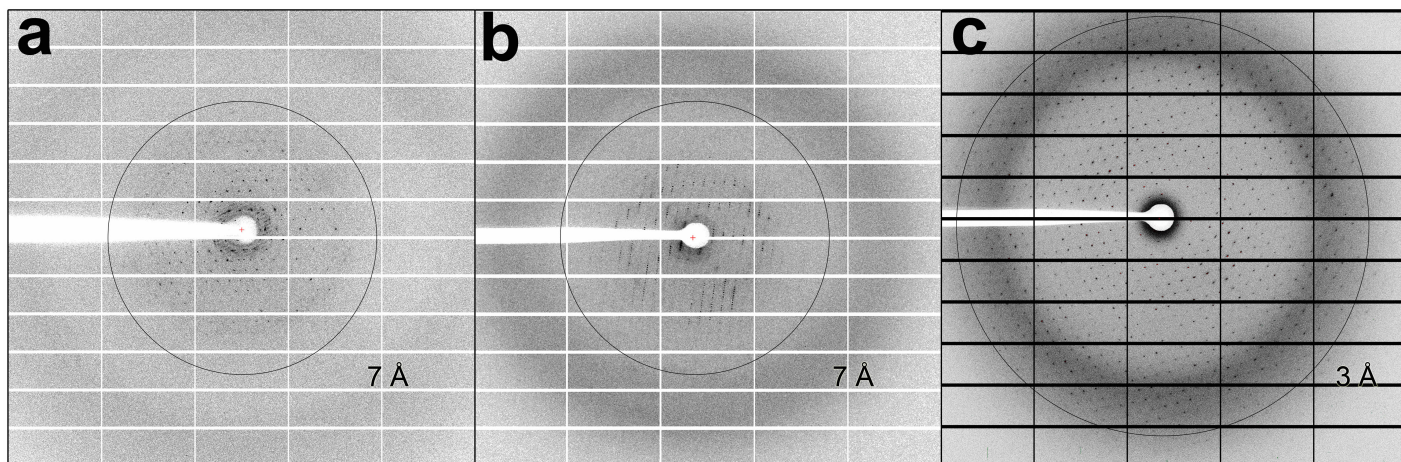


Fig. S2. Representative X-ray diffraction patterns. Diffraction images from crystals of (a) uncomplexed MdfA grown by the vapor diffusion method (**MdfA-VD**), (b) the MdfA-YN1074 complex grown by vapor diffusion (**MdfA-YN1074-VD**) and (c) the MdfA-YN1074 complex using the LCP method with 8.8 MAG (**MdfA-YN1074-LCP**).